Title: Wireframe DNA nanostructures from junction motifs

Authors: Kai Huang; Donglei Yang; Zhenyu Tan; Silian Chen; Ye Xiang; Yongli Mi; Chengde Mao; Bryan Wei

To be cited as: 10.1002/anie.201906408

Link to VoR: https://doi.org/10.1002/anie.201906408

Wireframe DNA nanostructures from junction motifs

Kai Huang[1], Donglei Yang[2, 3], Zhenyu Tan[1, †], Silian Chen[4, 5], Ye Xiang[4], Yongli Mi[2, 6], Chengde Mao[7, *], Bryan Wei[1, *]

[1]School of Life Sciences, Tsinghua University-Peking University Center for Life Sciences, Center for Synthetic and Systems Biology, Tsinghua University, Beijing 100084, China
[2]School of Chemical Science and Engineering, Tongji University, Shanghai 200092, China
[3]Institute of Molecular Medicine (IMM), Renji Hospital, Shanghai Jiao Tong University School of Medicine, Shanghai 200127, China
[4]Center for Infectious Disease Research, Collaborative Innovation Center for Diagnosis and Treatment of Infectious Diseases, Beijing Advanced Innovation Center for Structural Biology, Department of Basic Medical Sciences, School of Medicine, Tsinghua University, Beijing 100084, China
[5]School of Life Sciences, Peking University, Beijing 100084, China
[6]Department of Chemical and Biological Engineering, the Hong Kong University of Science and Technology, Kowloon, Hong Kong SAR
[7]Departmetn of Chemistry, Purdue University, West Lafayette, Indiana 47907, USA
*Corresponding author. Email: bw@tsinghua.edu.cn (B.W.); mao@purdue.edu (C.M.)
[†]Present address: Biophysics Program, University of Michigan, Ann Arbor, MI 48109, USA

Abstract

Wireframe framework has been investigated for construction of complex nanostructures from scaffolded DNA origami approach, but the similar framework is yet to be fully explored in scaffold-free 'LEGO' approach. Here we describe a general design scheme to construct wireframe DNA nanostructures entirely from short synthetic strands. A typical edge of the resulted structures in this study is composed of two parallel duplexes with crossovers on both ends, and three, four or five edges ray out from a certain vertex. We produce planar lattices and polyhedral objects according to such a self-assembly scheme.

Introduction

As a latecomer in DNA nanotechnology, scaffolded DNA origami method has showcased its self-assembly power and all kinds of complex structures have been constructed based on the method[1-8]. On the other hand, DNA self-assembly from short strands without the guidance from a scaffold, which was introduced to the field much earlier[9-17], has also emerged as a method for constructing complex addressable structures recently[18-20]. After a well-received introduction of complex addressable structures from single-stranded tiles/bricks, several classic motifs in DNA nanotechnology have been adopted to construct addressable nanostructures[21, 22]. The successful results have shown that the classic motifs are capable of self-assembly into not only micrometer periodic lattices with few repetitive motif species but also complex addressable structures with hundreds or even thousands of distinct motif species.

The structural motifs of this report are modified from those from earlier studies[22, 23]. Instead of regular lattice type (i.e. compact helices in parallel) of arrangement, armed motifs are designed to form lattice-free wireframe structures. To begin with, we use armed motifs to construct 2D wireframe structures of full addressability. Then we also demonstrate that single-stranded DNA (ssDNA) or double-stranded DNA (dsDNA) linkers at certain vertex can result in a desired angle control between the corresponding arms. Moreover, the similar designs are also applied to form extended structures from repetitive motifs. Besides planar wireframe structures, polyhedral objects, such as octahedron and icosahedron, are also constructed. The design principle presented in this study is a generally applicable to different types of addressable wireframe architectures.

Results

Different from the earlier designs, in which a typical double-duplex edge is bundled by crossovers in the middle of the helices[7, 8, 12, 16], a typical edge of all the structures presented in this study has two duplexes bundled by crossovers on both ends (i.e. crossovers at vertices).

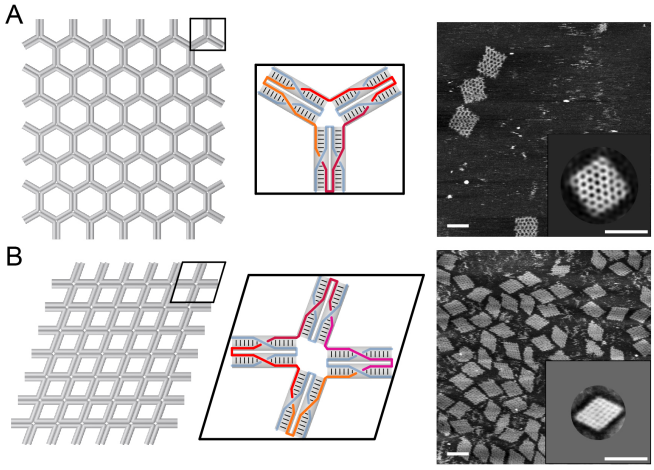

Figure 1. 2D addressable wireframe structures from armed motifs. (A) Addressable honeycomb grid with Y-shaped (3-arm) motifs. (B) Addressable rhombic grid with X-shaped (4-arm) motifs. Panels from left to right: schematic diagrams of full structures, schematic diagrams of representative motifs, and AFM images (scale bars: 100 nm). Insets show a reference-free class average calculated from single-particle AFM micrographs [N = 11 in (A) and N = 84 in (B)].

We first designed Y-shaped motifs to form an addressable honeycomb grid. The resulted honeycomb grid can be viewed as individual, virtual Y-shaped motifs intertwining with one another by their matching arms. A certain virtual Y-shaped motif is divided into three 52-nt strands, colored

differently (Figure 1A). Each component strand consists of four 13-nt domains (Figure S1). Each arm of a 'Y'-motif is paired by an arm from a matching 'Y'-motif for an edge of two bundled helices (each with 2.5 helical turns) with crossovers on both ends. The symmetric design ensures that there is only one nicking point for every component duplex. The full honeycomb grid consists of 77 distinct virtual 'Y'-motifs and there are 14 rows with five or six 'Y'-motifs for each row (256 distinct strands for the full structure). Similarly, we designed X-shaped motifs to form an addressable rhombic grid. Following the similar design principles, four nicking points correspond to four strands for each X-shaped virtual contour (each component strand is 52-nt long with four 13-nt domains) (Figure 1B and Figure S2). Individual virtual 'X'-motifs matching one another to form a rhombic grid composed of 42 'X'-motifs (seven rows by six columns; 194 distinctive strands for the full structure).

After agarose gel electrophoresis, a dominant band was presented for each addressable structure (including ones introduced later in this report), indicating a successful structural formation. Atomic force microscopy (AFM) images revealed the desired morphologies of honeycomb or rhombic grid with the expected dimensions and patterns (Figure 1, right panels). Detailed measurements can be found in Table S1. The formation of single 'Y'- and 'X'-motifs was characterized by agarose gel electrophoresis (Figure S3). Notably, the X-shaped motifs resulted in rhombic- instead of tetragonal-, shaped grids, and correspondingly the central cavity of the motif deformed from a square to a rhombus. An adjacent pair of angles of an X-shape vertex were ~110° and ~70°, instead of both 90°. It is presumably because of the compromise between two conflicting factors: maximizing base stacking between adjacent blunt ends at the vertices and minimizing electrostatic repulsion among the DNA backbones. Similar angle preferences have also been observed previously in other systems that involve 4-way branched motifs though exact angle values were different[24, 25].

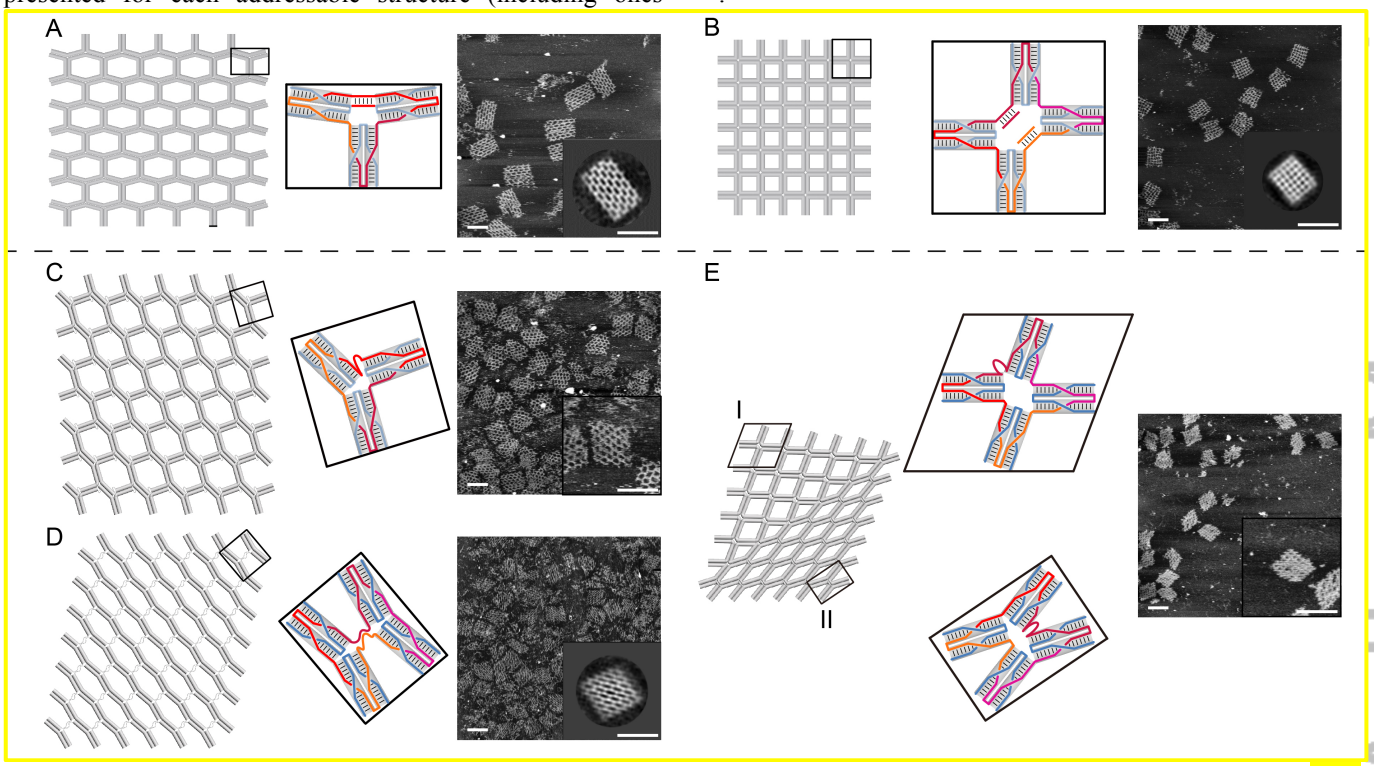

Figure 2. 2D addressable wireframe structures with angle control. (A) From Y-shaped vertices (Figure 1A) to T-shaped vertices (with double-stranded linker at one of the three crossover points of each vertex). (B) From X-shaped vertices (Figure 1B) to cross-shaped vertices (with double-stranded linkers at two of the four crossover points of each vertex). (C) From Y-shaped vertices (Figure 1A) to irregular 3-arm vertices (with single-stranded linker at one of the three crossover points of each vertex). (D) From X-shaped vertices (Figure 1B) to H-shaped vertices (with single-stranded linkers at two of the four crossover points of each vertex). (E) From X-shaped vertices (Figure 1B) to chimera vertices (with single-stranded linker at one of the four crossover points of each vertex). Panels from left to right: schematic diagrams of full wireframe structures, schematic diagrams of component motifs and AFM images (scale bars: 100 nm). Insets show reference-free class averages calculated from single-particle AFM micrographs [N = 15 in (A), N = 27 in (B) and N = 94 in (D)]. Averaging is not available for structures in C and E due to the particle heterogeneity.

For a 3-fold symmetric arrangement of the 'Y'-motif, the angles between any two arms are supposed to be 120° because the central cavity has an indeformable triangular shape. Indeed, ~120° angles were observed in the corresponding AFM image (Figure 1A). The observed value ~120° in the 'Y'-motif design was close to the observed value of ~110° in the 'X'-motif design, suggesting that similar local vertex structures between adjacent arms existed in both motifs. The geometry of the 'Y'-motif was subjected to adjustment. For example, when a 10-bp duplex segment was placed at one of the three crossover points between adjacent arms of a certain vertex, the geometry of the central cavity would change, leading an angle change from ~120° to ~150°. As a consequence, Y-shaped vertices deformed toward T-shaped (Figure 2A and Figure S4). Similar angle control was applied to X-shaped vertices of the rhombic lattice (Figure 2B and Figure S5). The incorporation of additional duplex segments (10 bp) led to an angle change from ~110°/~70° of the X-shaped vertices to ~90° of the cross-shaped vertices. (Figure 2B). As shown in averaged AFM images of structures with angle control (Figure 2, A and B, insets of right panels), the implementation strategy

was effective (Table S1). However, such a control was not precise and angles varied from junction point to junction point and from structure to structure. When the linker of each Y-shaped vertex was kept unpaired as ssDNA instead of dsDNA, the ~150° angles of the grid became less specified because of the unbalanced base stacking (Figure 2C; Figures S6 and S7). Self-assembly of the grids from 'X'-motifs with one or two 10-nt single-stranded linker(s) (three or two crossover points without linkers) at each vertex was also investigated. For an X-shaped vertex with two 10-nt single-stranded linker at crossover points of opposing positions, two pairs of adjacent arms without any linkers at the crossover points tended to have a strong base stacking interaction and the vertex became H-shaped. Hence a diagonal stripe pattern was presented for the grid (Figure 2D; Figure S6). Whereas, for an X-shaped vertex with one 10-nt single-stranded linker, the only 10-nt linker at a certain vertex induced a stacking orientation uncertainty. One of the two stacking orientations results in a specific local pattern. Consequently, a chimera of rhombic pattern and diagonal stripe pattern was presented for the grid (Figure 2E; Figure S6 and S7). The results with unpaired linkers clearly show that base stacking at the crossover point between adjacent arms can determine the general geometry of a vertex. The insertion of single-stranded linkers across arms weakens or cancels the stacking force and brings in flexibility to the corresponding vertex.

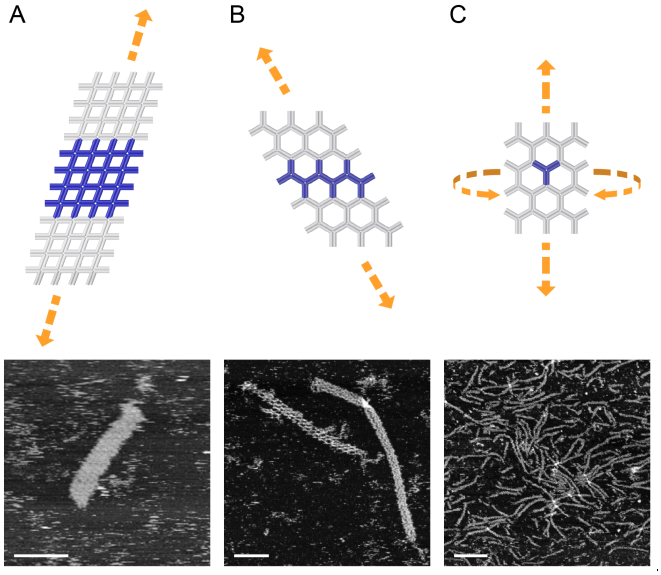

Figure 3. Extended wireframe structures from armed motifs. (A) Ribbon from 'X'-motifs extended in 1D. (B) Ribbon from 'Y'-motifs extended in 1D. (C) Tube structure from one continuous 'Y'-motif extended in 2D. Top: schematic diagrams (repetitive unit cells highlighted in blue); bottom: the corresponding AFM images (scale bars: 100 nm).

The same motifs were also implemented in a repetitive fashion for construction of extended structures. For example, a number of 'X'-motifs (4 × 4 array with 16 motifs) or 'Y'-motifs (2 × 3 array with 6 motifs) served as a repetitive unit cell for the construction of 1D extended ribbon. Samples after annealing were subjected to AFM imaging. 1D ribbons with desired widths and texture details under AFM shows the successful self-assembly (Figure 3, A and B; Figures S8 and S9). Especially, we designed one continuous strand consisting of six 16-nt domains (96-nt full length) as a full 'Y'-motif with palindromic segments and a tube structure was constructed entirely by one species of strand. Such a tubular configuration was verified under AFM (Figure 3C; Figure S10). Similar thin tubes were presented in other extended lattices with different numbers of repetitive motifs (Figures S11 and S12). Sparse nucleation of small flexible arrays in closed tubular conformation followed by fast growth would lead to the formation of thin tubes. We compared the self-assembly yields of the extended structures composed of different numbers of distinct motifs (i.e. different sizes of repetitive units) by agarose gel electrophoresis. The results revealed a yield decrease in self-assembly of increasing number of component strands (Figure S13).

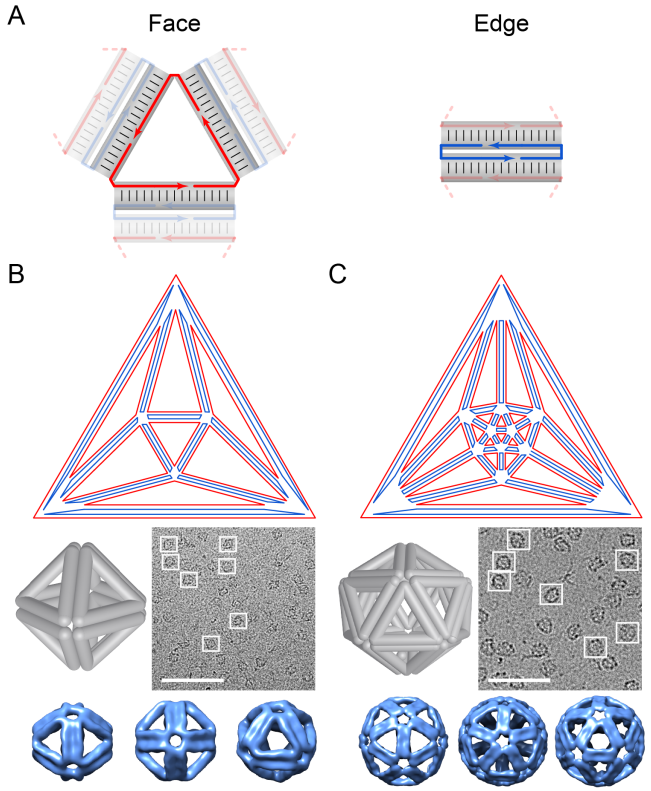

Figure 4. DNA polyhedra. (A) Schematic diagrams of the representative face and edge in a polyhedron. (B) DNA octahedron. (C) DNA icosahedron. In (B) and (C), Schlegel diagrams of polyhedra on top panels; cylinder models of polyhedra (left) and cryo-EM images on middle panels (scale bars: 100 nm); different views of 3D maps of DNA polyhedra reconstructed from cryo-EM images on the bottom panels.

Restricted by the polarity of DNA strands, it is not possible to use the same edge design (odd number of helical half-turns) for triangularly faced polyhedra such as octahedron and icosahedron[26] (Figures S14 and S15). Thus, we designed an octahedron and an icosahedron with two bundled DNA duplexes as edges, whose length was modified as even number of helical half-turns to satisfy polarity requirement. A DNA octahedron is composed of eight virtual triangles and twelve thin virtual rectangles (in each thin virtual rectangle, the two long edges depict two single stands of the corresponding duplexes and the two short edges depict phosphodiester bond). Two long sides of a thin rectangle are complementary to specific edges from two matching triangles to form a double-duplex edge of the DNA octahedron. As shown in Figure 4A, each triangle is composed of three DNA strands resulting from three nicks, and each thin rectangle is composed of two DNA strands resulting from two nicks. Because of the symmetric

arrangements, each DNA strand has three domains (11 nt, 10 nt and 11 nt, Figure S16). The single-stranded linker (i.e. T2) at each vertex of the triangle contour is designed to increase flexibility and the component strands have uniform lengths of 32/34 nt[7, 12, 16]. An octahedron of elongated edge length was also designed and constructed (Figure S17). As a control, component strands without T2 linkers (Figure S18) failed to self-assemble into a desired octahedron. The necessity to include linkers indicates that the flexibility of arms around a certain vertex associated from the linkers enables the arms to fit into a specific geometry. Similar design principles were also applied to construct a DNA icosahedron composed of twenty triangular contours and thirty thin rectangular contours.

The DNA polyhedra samples after gel-based purification were subjected to cryogenic transmission electronic microscopy (cryo-EM) for imaging. The desired morphologies of octahedron and icosahedron were presented after 3D reconstruction (Figure 4, B and C, bottom panels). The 3D maps also revealed that each edge was composed of two bundled duplexes. Also notably, the resolutions of the well-defined DNA polyhedra in this study are 1.9-2.5 nm (Figures S19-S21), which are comparable to ones constructed from repetitive motifs (at 1-4 nm resolutions)[16, 26-28]. In general, the limited resolution the 3D reconstruction of DNA polyhedra is presumably due to the structural flexibility and the corresponding sample inhomogeneity.

Discussion

Earlier examples in the field have shown that 2D lattices and 3D objects can be constructed by repetitive junction units[15, 16, 29-31]. In order to precisely control angles between arms, it is necessary to carefully design linker lengths around a certain vertex, and adjust the concentration of the component motifs especially in the formation of a certain type of polyhedron[16, 26, 30-32]. With precise molecular design, the minimalist strategy gives rise to extended 2D lattices of different patterns and a collection of polyhedra. On the other hand, most structures presented in this study are constructed with addressable components. In such a maximalist strategy, many more species of strands are involved and structural formation is deterministic without the necessity to fine tune strand concentrations and angles between junction arms.

Yields of nanostructures from maximalist strategy are in general low and a yield gap is apparent when counterparts from minimalist strategy are available (Table S2). As indicated by the yield decay for structures from increasing numbers of components (Figure S13 and Table S2), elevated complexity level could contribute to the difficulty of the desired self-assembly. On the other hand, the relative high yields in minimalist self-assembly can be attributed to a careful molecular design and construction (e.g. fine tuning of geometries of junction points and annealing protocols). Similar optimization could be applied to the maximalist self-assembly to achieve higher yields and better structural integrity. These two strategies can be viewed as two complementary design philosophies. The minimalist strategy requires less component strands but the molecular design to achieve precisely controlled geometries could be prohibitively challenging; the maximalist strategy enables greater structural complexity with simple molecular design, but requires synthesis of a large number of distinct DNA strands. The integration of the two strategies could lead to a cost-efficient construction of nanostructures of high complexity.

As the analogy of LEGO bricks in the macroscopic world goes, when bricks of different shapes and properties are included, one can build sophisticated models more easily. We believe the similar scenario applies to building blocks of structural DNA nanotechnology and that is the rationale behind our development to adopt different motifs, including ones in this study, to build complex DNA nanostructures[21, 22]. When building blocks of different fine structural features are available, one can build versatile DNA nanostructures with high level of controllability, precision and functionality.

Acknowledgements

We acknowledge the support from the Cryo-EM and Computing Platforms of the Tsinghua University Branch of the National Center for Protein Sciences (Beijing). Z.T. acknowledges support from Tsinghua Xuetang Life Science Program. This work is supported by National Natural Science Foundation of China grants (31770926 and 31570860), a 'Thousand Talents Program' Young Investigator Award, funds from Beijing Advanced Innovation Center for Structural Biology, and a startup fund from the Tsinghua University-Peking University Joint Center for Life Sciences to B.W., and an Office of Naval Research grant (N00014-15-1-2707) to C.M.

References

1. Rothemund, P. W., Folding DNA to create nanoscale shapes and patterns. *Nature* **2006,** *440* (7082), 297-302.
2. Dietz, H.; Douglas, S. M.; Shih, W. M., Folding DNA into Twisted and Curved Nanoscale Shapes. *Science* **2009,** *325* (5941), 725-730.
3. Douglas, S. M.; Dietz, H.; Liedl, T.; Hogberg, B.; Graf, F.; Shih, W. M., Self-assembly of DNA into nanoscale three-dimensional shapes. *Nature* **2009,** *459* (7245), 414-418.
4. Ke, Y.; Douglas, S. M.; Liu, M.; Sharma, J.; Cheng, A.; Leung, A.; Liu, Y.; Shih, W. M.; Yan, H., Multilayer DNA origami packed on a square lattice. *J Am Chem Soc* **2009,** *131* (43), 15903-15908.
5. Han, D.; Pal, S.; Nangreave, J.; Deng, Z.; Liu, Y.; Yan, H., DNA origami with complex curvatures in three-dimensional space. *Science* **2011,** *332* (6027), 342-346.
6. Benson, E.; Mohammed, A.; Gardell, J.; Masich, S.; Czeizler, E.; Orponen, P.; Hogberg, B., DNA rendering of polyhedral meshes at the nanoscale. *Nature* **2015,** *523* (7561), 441-444.
7. Zhang, F.; Jiang, S.; Wu, S.; Li, Y.; Mao, C.; Liu, Y.; Yan, H., Complex wireframe DNA origami nanostructures with multi-arm junction vertices. *Nat Nanotechnol* **2015,** *10* (9), 779-784.
8. Veneziano, R.; Ratanalert, S.; Zhang, K.; Zhang, F.; Yan, H.; Chiu, W.; Bathe, M., Designer nanoscale DNA assemblies programmed from the top down. *Science* **2016,** *352* (6293), 1534.
9. Seeman, N. C.; Kallenbach, N. R., Design of immobile nucleic acid junctions. *Biophys J* **1983,** *44* (2), 201-209.
10. Chen, J. H.; Seeman, N. C., Synthesis from DNA of a molecule with the connectivity of a cube. *Nature* **1991,** *350* (6319), 631-633.

11. Zhang, Y. W.; Seeman, N. C., Construction of a DNA-Truncated Octahedron. *Journal of the American Chemical Society* **1994,** *116* (5), 1661-1669.
12. Yan, H.; Park, S. H.; Finkelstein, G.; Reif, J. H.; LaBean, T. H., DNA-templated self-assembly of protein arrays and highly conductive nanowires. *Science* **2003,** *301* (5641), 1882-1884.
13. Goodman, R. P.; Schaap, I. A.; Tardin, C. F.; Erben, C. M.; Berry, R. M.; Schmidt, C. F.; Turberfield, A. J., Rapid chiral assembly of rigid DNA building blocks for molecular nanofabrication. *Science* **2005,** *310* (5754), 1661-1665.
14. Malo, J.; Mitchell, J. C.; Venien-Bryan, C.; Harris, J. R.; Wille, H.; Sherratt, D. J.; Turberfield, A. J., Engineering a 2D protein-DNA crystal. *Angewandte Chemie-International Edition* **2005,** *44* (20), 3057-3061.
15. He, Y.; Tian, Y.; Ribbe, A. E.; Mao, C. D., Highly connected two-dimensional crystals of DNA six-point-stars. *Journal of the American Chemical Society* **2006,** *128* (50), 15978-15979.
16. He, Y.; Ye, T.; Su, M.; Zhang, C.; Ribbe, A. E.; Jiang, W.; Mao, C. D., Hierarchical self-assembly of DNA into symmetric supramolecular polyhedra. *Nature* **2008,** *452* (7184), 198-201.
17. Zheng, J.; Birktoft, J. J.; Chen, Y.; Wang, T.; Sha, R.; Constantinou, P. E.; Ginell, S. L.; Mao, C.; Seeman, N. C., From molecular to macroscopic via the rational design of a self-assembled 3D DNA crystal. *Nature* **2009,** *461* (7260), 74-77.
18. Ke, Y.; Ong, L. L.; Shih, W. M.; Yin, P., Three-dimensional structures self-assembled from DNA bricks. *Science* **2012,** *338* (6111), 1177-1183.
19. Wei, B.; Dai, M.; Yin, P., Complex shapes self-assembled from single-stranded DNA tiles. *Nature* **2012,** *485* (7400), 623-626.
20. Ong, L. L.; Hanikel, N.; Yaghi, O. K.; Grun, C.; Strauss, M. T.; Bron, P.; Lai-Kee-Him, J.; Schueder, F.; Wang, B.; Wang, P.; Kishi, J. Y.; Myhrvold, C.; Zhu, A.; Jungmann, R.; Bellot, G.; Ke, Y.; Yin, P., Programmable self-assembly of three-dimensional nanostructures from 10,000 unique components. *Nature* **2017,** *552* (7683), 72-77.
21. Wang, W.; Lin, T.; Zhang, S.; Bai, T.; Mi, Y.; Wei, B., Self-assembly of fully addressable DNA nanostructures from double crossover tiles. *Nucleic Acids Res* **2016,** *44* (16), 7989-7996.
22. Yang, D.; Tan, Z.; Mi, Y.; Wei, B., DNA nanostructures constructed with multi-stranded motifs. *Nucleic Acids Research* **2017,** *45* (6), 3606-3611.
23. Liu, H. P.; Chen, Y.; He, Y.; Ribbe, A. E.; Mao, C. D., Approaching the limit: Can one DNA oligonucleotide assemble into large nanostructures? *Angewandte Chemie-International Edition* **2006,** *45* (12), 1942-1945.
24. Cui, Y.; Chen, R.; Kai, M.; Wang, Y.; Mi, Y.; Wei, B., Versatile DNA Origami Nanostructures in Simplified and Modular Designing Framework. *ACS Nano* **2017,** *11* (8), 8199-8206.
25. Song, J.; Li, Z.; Wang, P.; Meyer, T.; Mao, C.; Ke, Y., Reconfiguration of DNA molecular arrays driven by information relay. *Science* **2017,** *357* (6349), eaan3377.
26. Wang, P.; Wu, S.; Tian, C.; Yu, G.; Jiang, W.; Wang, G.; Mao, C., Retrosynthetic Analysis-Guided Breaking Tile Symmetry for the Assembly of Complex DNA Nanostructures. *J Am Chem Soc* **2016,** *138* (41), 13579–13585.
27. Zhang, C.; Su, M.; He, Y.; Zhao, X.; Fang, P.-a.; Ribbe, A. E.; Jiang, W.; Mao, C., Conformational flexibility facilitates self-assembly of complex DNA nanostructures. **2008,** *105* (31), 10665-10669.
28. He, Y.; Su, M.; Fang, P. A.; Zhang, C.; Ribbe, A. E.; Jiang, W.; Mao, C., On the chirality of self-assembled DNA octahedra. *Angew Chem Int Ed Engl* **2010,** *49* (4), 748-751.
29. Liu, D.; Wang, M.; Deng, Z.; Walulu, R.; Mao, C., Tensegrity: construction of rigid DNA triangles with flexible four-arm DNA junctions. *J Am Chem Soc* **2004,** *126* (8), 2324-2325.
30. He, Y.; Chen, Y.; Liu, H. P.; Ribbe, A. E.; Mao, C. D., Self-assembly of hexagonal DNA two-dimensional (2D) arrays. *Journal of the American Chemical Society* **2005,** *127* (35), 12202-12203.
31. He, Y.; Tian, Y.; Chen, Y.; Deng, Z. X.; Ribbe, A. E.; Mao, C. D., Sequence symmetry as a tool for designing DNA nanostructures. *Angewandte Chemie-International Edition* **2005,** *44* (41), 6694-6696.
32. Liu, L.; Li, Z.; Li, Y.; Mao, C., Rational Design and Self-Assembly of Two-Dimensional, Dodecagonal DNA Quasicrystals. *Journal of the American Chemical Society* **2019,** *141* (10), 4248-4251.